ISSN: 0976-0172

Journal of Bioscience And Technology
www.jbstonline.com

Robustness Analysis and Improvement of Phase Retrieval Algorithms Through Visualization

Mr.K.Naresh[1]., M.Mounika[2]

1 Assistant Professor, Department of CSE, Malla Reddy College of Engineering for Women., Maisammaguda., Medchal., TS, India

2, B.Tech CSE (21RG5A0520),

Malla Reddy College of Engineering for Women., Maisammaguda., Medchal., TS, India

Article Info

Received: 31-09-2023 *Revised: 20-11-2023* *Accepted: 30-11-2023*

Abstract

To picture matter on the nanoscale scale, a revolutionary imaging technology called coherent x-ray diffractive imaging uses phase retrieval and nonlinear optimization techniques. By introducing a reduced dimensionality issue, we are able to observe and quantitatively assess the convergence to local minima and the globally optimum solution of a well-known phase retrieval approach, Fienup's HIO. Next, we provide extensions to HIO that boost the original algorithm's convergence to the global optimum.

Introduction

Imaging a sample without the need of optics is possible using coherent x-ray diffractive imaging (CXDI) [9]. In the experimental geometry shown in Fig. 1, monochromatic coherent plane wave x-rays interact with a sample to form an exit wave ρ(r) ∈ Cm×n, where r ∈ R = {(ru, rv): u ∈ 0, . . . , n−1, v ∈ 0, . . . , m−1} denotes a length scale that is the spatial resolution of the microscope and mn ∈ Z is the number of complex variables constituting the measured exit wave. To do this, we position a detector in the far field and measure the amount F [], which is proportional to the squared modulus of the Fourier transform of the exit wave. The resulting diffraction pattern, expressed as a function of frequency, is given by D = |F[] |2 + Rmn +, where | |2 is the squared modulus |a|2 = a_a, where is the complex conjugate and _ is the Hadamard (component wise) product for any a Cmn. By measuring the coherent diffraction pattern D Rmn +, for instance using nonlinear optimization methods, CXDI hopes to recover the discrete representation of the exit wave, Cmn. The "phase problem," caused by x-ray area detectors' inability to measure a whole complex-valued wave field, is circumvented by this method. tan1 (Im () Re ()) (with the divided component) is recovered, which is the missing phase.

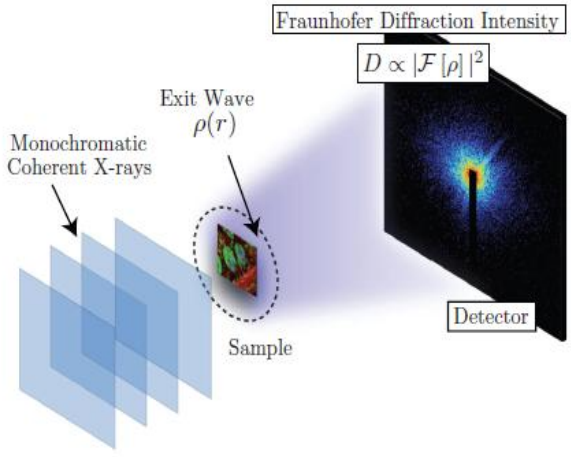

Experiment using CXDI shown in Figure 1. What is observed is proportional to the squared modulus of the Fourier transform of the exit wave when monochromatic coherent plane-wave x-rays interact with a sample and a detector is situated in the far

ISSN: 0976-0172

Journal of Bioscience And Technology
www.jbstonline.com

field. The number of pixels in the area detector is what gives the measurement its mn size. Insightful), begins with a first estimate for the exit wave and refines the current exit wave iteration using information gathered from the experiment. In addition to the observed diffraction intensities D, this data also contains information about the sample itself, such as the support of the sample, which characterizes an area in the space R in which the sample is known not to exist. Since its first implementation, CXDI has been used to a wide variety of sample types and experimental settings, where it has been proven to produce a novel exit wave under certain conditions [1, 3, 11, 9]. When the recovered exit wave fulfills restrictions specified by, then the issue of CXDI may be seen as a feasibility problem [2], locate some S M, (1).

the collection of spatial indices S R that corresponds to the sample's backing. The intensity of the observed coherent diffraction pattern serves as the basis for the measurement constraint set M, which is defined as

When the multiplication _ and division ÷ are component wise: .
We may provide projection operators for both sets S and M.

The alternating projection approach, often known as "error reduction" (ER) in the phase retrieval community [5] is one of the simplest algorithms for roughly solving (1).

See Figure 2a for an illustration of how the ER algorithm continually moves back and forth between the sample space and the diffraction space by applying the measurement projection M and the support projection S. Since ER may be thought of as the problem's expected sharpest decline,

Trajectory #1 in Fig. 2b shows that it may become stuck at stationary sites that do not solve (1). Our numerical findings confirm that the initial prediction for the exit wave is crucial to the final outcome of the convergence process.(0). Although numerous approaches have been devised to break through this impasse, the "hybrid input-output" (HIO) approach proposed by Fienup [5] is now the workhorse of experimentalists. By adjusting the relaxation parameter R, HIO may be seen as a variant of the Douglas-Rachford method for nonconvex problems [2]:

where Sc = Cmn: / S0 and S + Sc = 1, with 1 Rmn signifying the matrix containing all ones; Sc is an orthogonal binary operator to S. Numerical findings reveal that HIO is superior than ER at preventing stagnation at nonglobal solutions. However, it will be shown that more resilient algorithms do exist. This paper makes the following contributions. To improve HIO's efficacy and robustness while escaping from nonglobal solutions, we investigate extended formulations of HIO as a saddle-point optimization problem and provide optimization-based ways to do so. We present a technique for visualizing a low-dimensional issue such that one may get a feel for the saddle-point target and how an algorithm can move across the space to reach it. We next have a look at the HIO variations that have been created using this method.

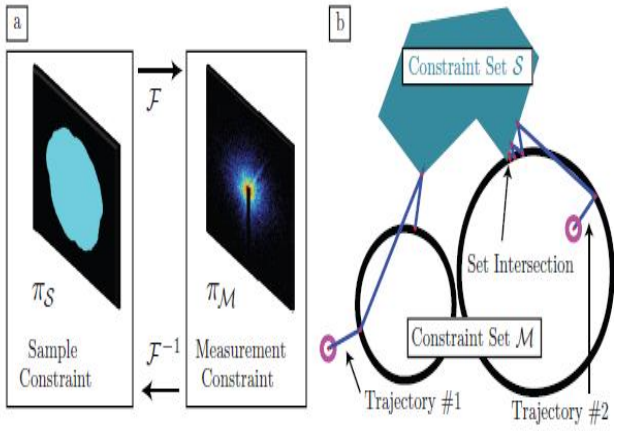

As shown in Figure 2(a), regular CXDI algorithms use restrictions on both the sample and diffraction-space representations, as well as the Fourier and inverse Fourier transforms. (b) The effectiveness of CXDI algorithms is sensitive to the value of (0), with various initializations yielding distinct trajectories.

HIO and the Optimization of the Saddle Point

As a heuristic for locating a Nash equilibrium (for an example, see [4]), the HIO technique in (5) may be thought of.

$$\min_{\rho_s \in \mathcal{S}} \quad \mathcal{L}(\rho_s + \rho_{\underline{s}})$$
$$\max_{\rho_{\underline{s}} \in \mathcal{S}^c} \quad \mathcal{L}(\rho_s + \rho_{\underline{s}}),$$

ISSN: 0976-0172

Journal of Bioscience And Technology
www.jbstonline.com

Where

$$\rho_s = \pi_{\mathcal{S}}\rho \text{ and } \rho_{\underline{s}} = \pi_{\mathcal{S}^c}\rho = (\mathbf{1} - \pi_{\mathcal{S}})\rho$$

Represent an orthogonal decomposition of

$$\mathbb{C}^{m\times n}$$

The objective function

$$\mathcal{L} : \mathbb{C}^{m\times n} \to \mathbb{R}$$

Is given by

$$\mathcal{L}(\rho) = \varepsilon^2_{\mathcal{M}}(\rho) - \varepsilon^2_{\mathcal{S}}(\rho) = \|\pi_{\mathcal{M}}\rho - \rho\|^2_F - \|\pi_{\mathcal{S}}\rho - \rho\|^2_F.$$

In this game, one player seeks to minimize the objective by controlling ρ inside the support, while The second player seeks to maximize the objective by controlling ρ outside the support. Nash equilibrium for (6) correspond to particular saddle points of the function $f(\rho_s, \rho_{\underline{s}}) = \mathcal{L}(\rho_s + \rho_{\underline{s}})$. this fact motivates algorithmic approaches that solve related saddle-point problems [7].

Two-Dimensional Search and HIO Generalizations

Using Wirtinger calculus

$$\left(\text{where } \nabla_{\bar{\rho}} = \frac{\partial}{\partial\bar{\rho}} = \frac{1}{2}\left(\frac{\partial}{\partial \text{Re}(\rho)} + i\frac{\partial}{\partial \text{Im}(\rho)}\right);\right.$$

see [10]), we compute the gradient of (7) with respect

$$\nabla_{\bar{\rho}}\mathcal{L}(\rho) = (\pi_{\mathcal{S}} - \pi_{\mathcal{M}})\rho.$$

This (complex-valued) gradient can be decomposed into parts inside and outside the support, respectively:

$$\delta_s = \pi_{\mathcal{S}}\nabla_{\bar{\rho}}\mathcal{L}(\rho) = (\pi_{\mathcal{S}} - \pi_{\mathcal{S}}\pi_{\mathcal{M}})\rho$$

and

$$\delta_{\underline{s}} = \pi_{\mathcal{S}^c}\nabla_{\bar{\rho}}\mathcal{L}(\rho) = -\pi_{\mathcal{S}^c}\pi_{\mathcal{M}}\rho,$$

where we have used the fact that

$$\pi_{\mathcal{S}^c}\pi_{\mathcal{S}} = \mathbf{0},\ \pi_{\mathcal{S}}\pi_{\mathcal{S}} = \pi_{\mathcal{S}},$$

and where

$$\mathbf{0} \in \mathbb{R}^{m\times n}$$

s

i the matrix containing all zeros. Taking a step along the steepest descent direction inside the support and a step along the steepest ascent direction outside the support would thus correspond to the combined direction

$$(-\delta_s, \delta_{\underline{s}}).$$

If we allow for unequal steplengths (α, β) along these respective orthogonal directions, we obtain the first-order update

$$\rho^{(k+1)} = \rho^{(k)} - \alpha\delta_s^{(k)} + \beta\delta_{\underline{s}}^{(k)} = (1-\alpha)\rho^{(k)} + \alpha(\pi_{\mathcal{S}}\pi_{\mathcal{M}})\rho^{(k)} + \pi_{\mathcal{S}^c}(\alpha 1 - \beta\pi_{\mathcal{M}})\rho^{(k)},$$

where we have used the fact that

$$\pi_{\mathcal{S}} + \pi_{\mathcal{S}^c} = \mathbf{1}.$$

The HIO method of then applies only when = 1. (5). Going beyond the = 1 situation and considering more generic values for yields a generalization of the HIO method, as opposed to utilizing a fixed value drawn from the normal range of [0.5, 1] as is imposed by real HIO implementations [5, 7]. Solving the two-dimensional version of (6) with the same goal in mind may be used to generate the (,) values needed for each iteration of the form (9).

$$\psi_k(\alpha,\beta) = \mathcal{L}(\rho^{(k)} - \alpha\delta_s^{(k)} + \beta\delta_{\underline{s}}^{(k)}).$$

Using the notation

$$\frac{\partial}{\partial a} = \partial_a \text{ and } \frac{\partial^2}{\partial a\partial b} = \partial_{ab},$$

we desire (α, β) such that $\partial_\alpha\psi_k(\alpha,\beta) =$

$$\partial_\beta\psi_k(\alpha,\beta) = 0 \text{ and } \partial_{\alpha\alpha}\psi_k(\alpha,\beta) \geq 0 \geq \partial_{\beta\beta}\psi_k(\alpha,\beta).$$

One approach is to use a modified Newton method for the problem $\min_{\alpha,\beta}\Phi_k(\alpha,\beta)$:

$$\begin{bmatrix}\alpha_{j+1}\\ \beta_{j+1}\end{bmatrix} = \begin{bmatrix}\alpha_j\\ \beta_j\end{bmatrix} - \mu\begin{bmatrix}|\partial_{\alpha\alpha}\psi_k(\alpha_j,\beta_j)| & \partial_{\alpha\beta}\psi_k(\alpha_j,\beta_j)\\ \partial_{\beta\alpha}\psi_k(\alpha_j,\beta_j) & -|\partial_{\beta\beta}\psi_k(\alpha_j,\beta_j)|\end{bmatrix}^{-1}\begin{bmatrix}\partial_\alpha\psi_k(\alpha_j,\beta_j)\\ \partial_\beta\psi_k(\alpha_j,\beta_j)\end{bmatrix},$$

Where

$$\Phi_k(\alpha,\beta) = \|\nabla\psi_k(\alpha,\beta)\|^2 = |\partial_\alpha\psi_k(\alpha,\beta)|^2 + |\partial_\beta\psi_k(\alpha,\beta)|^2.$$

Minimization and maximizing with regard to are both possible given the right choice of second-order matrix form in (10). For the aim k(,), a line search

ISSN: 0976-0172

Journal of Bioscience And Technology
www.jbstonline.com

(for example, with the strong Wolfe conditions) may be used to find the step length ; a similar technique is utilized in [7]. Fig. 3 depicts a typical instance of this procedure.

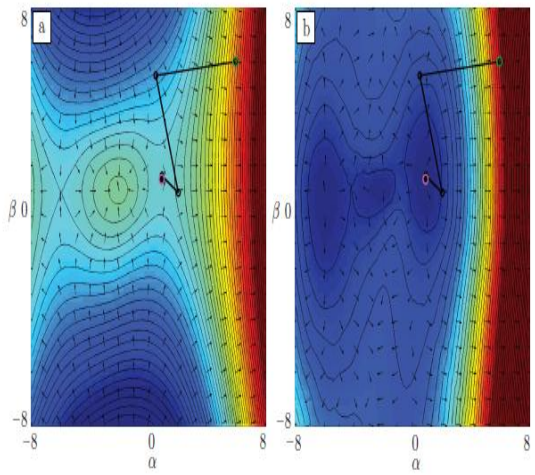

Optimization of both and by locating a specific saddle point of k(,) is seen in Figure 3. Two contour plots, one for each of the functions k(,) and k(,). The trajectory computed using the modified Newton step in (10) is superimposed on both graphs; the green circle represents the starting position (0, 0), and the magenta circle represents the ending position (5, 5). (after 5 iterations).

Quasi-Newton and Conjugate Gradient Update Directions

HIO is a specific instance of the bidirectional strategy mentioned above, but other, more general strategies for problem resolution are also possible. (6). We now suggest two such methods that make use of general directions dk in the update and are based, respectively, on L-BFGS and conjugate gradient (CG) direction steps.

$$\rho^{(k+1)} = \rho^{(k)} + \alpha_k d_{\underline{s}}^{(k)} + \beta_k d_{\underline{s}}^{(k)}, \qquad k = 0, 1, \ldots,$$

instead of the gradient directions prescribed by (8) and (9). In all the results that follow, we initialize

$$d_{\underline{s}}^{(0)} = -\delta_{\underline{s}}^{(0)} \text{ and } d_{\underline{s}}^{(0)} = \delta_{\underline{s}}^{(0)}.$$

In most experimental contexts, the number of complex-valued variables in a phase retrieval issue is on the order of mn = 106. In order to employ the dense Hessian (with 1012 complex-valued variables) in quasi-Newton techniques, it is too costly in terms of storage to compute an approximation of the Hessian. To get around this, we turn to L-BFGS [8] and other limited-memory approaches. Algorithm 1 presents our L-BFGS approach, which is based on recent work by [10].

For the sake of explanation, we'll assume that you're familiar with how vectors operate and that the numbers sk1, yk1, and gk are all column vectors in the vectorized form, Cmn. With the right projection (S or Sc), Algorithm 1 may be utilized either within (A = S) or outside (A = Sc) the support. Our implementation remembers the previous p = 5 changes. In the first algorithm, the desired minimum or maximum is determined by the inertia of the quasi-Newton Hessian Bk. By appropriately scaling the original quasi-Newton matrix (in our studies, we utilize the identity matrix), we are able to obtain the desired orientation. The conditional

$$\frac{\langle \mathbf{y}_{k-1}, \mathbf{s}_{k-1} \rangle}{\|\mathbf{y}_{k-1}\|^2} = \frac{\mathbf{Re}[\ \mathbf{y}_{k-1}^H \mathbf{s}_{k-1}\ ]}{\mathbf{Re}[\ \mathbf{y}_{k-1}^H \mathbf{y}_{k-1}\ ]}$$

Input: $g_k = \pi_A \nabla_{\tilde{\rho}} \mathcal{L}(\rho^{(k)}), \left\{ \left(y_j = g_{j+1} - g_j, \quad s_j = \pi_A \left(\rho^{(j+1)} - \rho^{(j)} \right) \right) \right\}_{j=\max\{0,k-p\}}^{j=k-1}, p \geq 1.$

Output: $d^{(k)} = -d = -B_k^{-1} \nabla_{\tilde{\rho}} \mathcal{L}(\rho^{(k)})$

$d \leftarrow g_k$

for $j = k-1, \ldots, \max\{0, k-p\}$ do

$\varrho_j \leftarrow (\langle y_j, s_j \rangle)^{-1}; \quad \nu_j \leftarrow \varrho_j \langle s_j, d \rangle; \quad d \leftarrow d - \nu_j y_j$

end for

$d \leftarrow \frac{\langle y_{k-1}, s_{k-1} \rangle}{\|y_{k-1}\|^2} d$

for $j = \max\{0, k-p\}, \ldots, k-1$ do

$\xi \leftarrow \varrho_j \langle y_j, d \rangle; \quad d \leftarrow d + (\nu_j - \xi) s_j$

end for

If (12) in the first algorithm, where H is the ermitian transposition, is positive, the quasi-Newton step is returned in the downhill direction, and in the uphill direction if (12) is negative. We also take into account nonlinear CG directions of the kind

$$d_{\underline{s}}^{(k+1)} = -\delta_{\underline{s}}^{(k+1)} + \gamma_{\underline{s}}^{(k+1)} d_{\underline{s}}^{(k)} \quad \text{and} \quad d_{\underline{s}}^{(k+1)} = \delta_{\underline{s}}^{(k+1)} + \gamma_{\underline{s}}^{(k+1)} d_{\underline{s}}^{(k)}, \quad k = 0, 1, \ldots, \quad (13)$$

ISSN: 0976-0172

Journal of Bioscience And Technology
www.jbstonline.com

With δ_s and $\delta_{\underline{s}}$ defined from (8). Several lternatives for the CG parameter γ exist (see, e.g., [6]), and we consider the seven variants listed in Table 1. We employ separate updates for the Variables

$$\rho_s \text{ and } \rho_{\underline{s}}, \text{ so that } \gamma_s^{(k)} \ (\gamma_{\underline{s}}^{(k)}) \text{ is}$$

determined by using

$$\mathbf{g}_k = \delta_s^{(k)} \ (\mathbf{g}_k = -\delta_{\underline{s}}^{(k)})$$

and

$$\mathbf{d}_k = d_s^{(k)} \ (\mathbf{d}_k = d_{\underline{s}}^{(k)}).$$

These two sets of choices are made based on whether we are updating in *S* (minimizing) or in *Sc* (maximizing).

Numerical Experiments with HIO Variants

We now examine the effectiveness of the methods escribed in Sec. 2 in terms of their robustness for solving the low-dimensional problem whose exit wave

$$\rho \in \mathbb{R}^{16\times 16}$$

and diffraction pattern

$$D \in \mathbb{R}_+^{16\times 16}$$

+ are shown in Figs. 4a and 4b, respectively. The exit wave is real-valued and consists of three pixels,

$$\rho(r_a) = 0.05, \ \rho(r_b) = 0.8, \text{ and } \rho(r_c) = 0.125$$

arranged in an upside-down-L shape. The remaining pixels are zero, and the correct support

$$S = \{r_a, r_b, r_c\}$$

Fletcher-Reeves (FR):	$\gamma = \frac{\|g_{k+1}\|^2}{\|g_k\|^2}$	Polak-Ribière (PR):	$\gamma = \frac{\langle g_{k+1}, y_k\rangle}{\|g_k\|^2}$
Hestenes-Stiefel (HS):	$\gamma = \frac{\langle g_{k+1}, y_k\rangle}{\langle d_k, y_k\rangle}$	Liu-Storey (LS):	$\gamma = \frac{\langle g_{k+1}, y_k\rangle}{\langle -d_k, g_k\rangle}$
Dai-Yuan (DY):	$\gamma = \frac{\|g_{k+1}\|^2}{\langle d_k, y_k\rangle}$	Conjugate Descent (CD):	$\gamma = \frac{\|g_{k+1}\|^2}{\langle -d_k, g_k\rangle}$
Hager-Zhang (HZ):	$\gamma = \frac{\left\langle y_k - 2d_k \frac{\|y_k\|^2}{\langle d_k, y_k\rangle}, g_{k+1}\right\rangle}{\langle d_k, y_k\rangle}$		

Table 1: CG parameter expressions for the algorithms considered .we define

$$\mathbf{y}_k = \mathbf{g}_{k+1} - \mathbf{g}_k,$$
$$\|a\|^2 = \langle a, a\rangle,$$

and the inner product

$$\langle a, b\rangle = e^T \mathrm{Re}[\ \bar{a} \odot b\ ]e,$$

where e is a standard vector consisting only of ones. For the sake of illustration, we will pretend that rc is already known; this will leave us with a problem that has 255 complex variable dimensions, with the only two nonzero values being

$$: \rho(r_a) \text{ and } \rho(r_b),$$

a scenario that was conceived after reading [7], which had a comparable synthetic dilemma. Because of this dilemma, we are able to see the solution in a subspace that only has two dimensions.

$$(\rho(r_a), \rho(r_b),$$
$$\rho(r_c) = 0.125, \rho_{\underline{s}} = 0) \text{ where } \mathcal{L}(\rho)$$

reduces to the the modulus objective function

$$\varepsilon_{\mathcal{M}}^2(\rho) = \|\pi_{\mathcal{M}}\rho - \rho\|_F^2$$

depending on the values of ra and rb; see Fig. 4c. The input exit wave (with (ra) = 0.05 and (rb) = 0.8) corresponds to the global minimum labeled mG of this measure. Due to the fact that phase retrieval is often insensitive to global phase changes in the exit wave (i.e.,

$$|\mathcal{F}[\rho]| = |\mathcal{F}[\rho e^{i\phi_0}]|$$

for a fixed 0 R phase difference. At the m1 minimum, the input exit wave ((ra) = 0.05 and (rb) = 0.8)

ISSN: 0976-0172

Journal of Bioscience And Technology
www.jbstonline.com

exhibits a negative phase shift of 0 =. Since the value of (rc) is known, however, such worldwide phase shifts are not comparable in our issue. Because of symmetry in the Fourier transform, the non-global minima denoted by the labels m2 and m3 appear when is rotated by 180 degrees. Minimum m2 corresponds to a 180-degree rotation of the exit wave, and minimum m3 corresponds to a 180-degree rotation of the exit wave. Knowing the value of breaks the symmetry of the Fourier transform, making the m2 and m3 minima non-global in the same way that m1 is.(rc). Based on this issue formulation, we offer a way of representing the exit wave retrieved as a function of the initial conditions of the process ((0)(ra), (0)(rb)). Starting from the box [1.5, 1] with increments of 0.15, we evaluate 441 initial values ((0)(ra), (0)(rb))..5]2. From this chosen initial point, we next check to see which of the 2 M minima (mG, m1, m2, or m3) in the two-dimensional space ((ra), (rb)) the technique converges to. Fig. 4d depicts such an illustration for the ER technique from (4). The ER approach is projected steepest descent; therefore we anticipate returning to the inima that is geographically closest to the origin. The derived minimum is highlighted in green at the origin in Fig. 4d, confirming the validity of this finding. With careful attention paid to maintaining constant experimental circumstances, we do these 441 runs again using an implementation of each of the provided techniques. For our initial (0), everything is set to zero except for the predetermined values for ra and rb and the constant rc. Each of the new variations updates (1) in the same way as in Sec. 2.1, but they start with different beginning search directions: d(0) s = (0) s and d(0) s = (0) s. (11). To determine the next set of search directions d, we apply the L-BFGS or CG update to calculate L((k)).(k). After this revision is complete, we'll find the optimum (k, k) and revise k+1. After computing d(k) at each iteration, we check the sign on the directional derivatives in S and Sc by computing Re[_ r[(k) _ d(k)](r)]; if we have a positive directional derivative when updating in S (going uphill when we should be going down) or a negative directional derivative when updating in Sc (going downhill when we should be going up), we reset the offending update to be the standard HIO update Only five rounds of the saddle-point optimization method are permitted for identifying optimum (k, k). (10). Using the optimum (,) and search directions inside and outside the support provided in (8), we see in Fig. 4e that the HIO approach from (9) can escape the local minima m2 and m3, but it is vulnerable to stagnation in the nonglobal minimum m1. About 75% of the time, out of a total of 441 possible initializations, HIO with optimum (,) can locate the global minimum mG. Results for illustrative combinations of CG and L-BFGS within and outside the support with (,) are shown in Fig. 4f-i. Some combinations of CG search directions and DY update (Table 1) within the support and FR update (Table 1) outside the support are obvious, as shown in Fig. 4f.

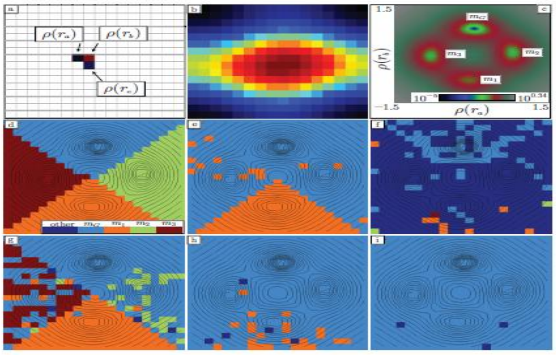

Figure 4: (a) The exit wave $\rho(r) \in$ R16×16 used. It is assumed that the bottom pixel (rc) is known but the top two pixels (ra, rb) are not. The diffraction pattern for the exit wave in (b) (a). This section demonstrates how to calculate the modulus objective function 2 M() = M 2 F using brute force, given that there are only two unknowns ((ra), (rb)). (d) Attempting to solve the phase issue by using the local minimizer ER (projected steepest descent); depending on the initial condition, we will arrive at the nearest of the four minima mG, m1, m2, and m3. Saddle-point optimization is used to converge to these minima, yielding the best (,) and (e) canonical HIO directions. (8). Using (f) Dai-Yuan in S and (g) Fletcher-Reeves in Sc are two examples of when CG update paths lead to a poorer result. Hager-Zhang in S and Polak Ribi'ere in Sc significantly enhance the outcome in (e). (i) We are able to locate mG from practically any initial location (99% success rate) by using L-BFGS in S and Hestenes-Steifel in Sc.

ISSN: 0976-0172

Journal of Bioscience And Technology
www.jbstonline.com

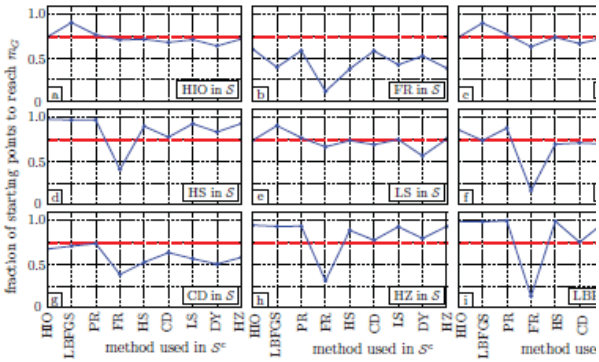

Using combinations of the standard HIO directions (Figure 5), the CG direction updates (Table 1), and the L-BFGS direction updates (Figure 5), we can see what percentage of initial points had their global inimum mG regained. (Algorithm 1). (a) Using the optimum (,) in conjunction with direction updates outside the support, as opposed to using regular HIO direction updates from (9). Comparison of Fletcher-Reeves (FR), Polak-Ribi'ere (PR), Hestenes-Steifel (HS), Liu-Storey (LS), Dai-Yuan (DY), Conjugate Descent (CD), Hager-Zhang (HZ), and L-BFGS (i) direction updates within the support and outside the support. The red dotted line represents the proportion of times the global minimum was obtained when standard HIO was used inside and outside of the support in addition to the optimum (,). There are major drawbacks to CG updates both within and outside the support. With the LS update within the support and the DY update outside the support, as shown in Fig. 4g, the negative impacts of using the CG update parameters are mitigated compared to Fig. 4f. Using the L-BFGS direction update from (1) inside the support and the HS update from Table 1 outside the support, as shown in Fig. 4h, and the HZ update inside the support and the PR update outside the support, as shown in Fig. 4i, are two examples of CG and L-BFGS update combinations that significantly improve the algorithm's beneficial ability to converge to the global solution. Results for the 81 versions generated by coupling various methods for both internal and external updates are summarized in Fig. 5. The charts reveal what percentage of the interval's 441 beginning locations provide the global minimum mG. These findings allow us to evaluate whether or not combining L-BFGS with CG direction updates in S and Sc yields more stable performance. When compared to the typical HIO update in Fig. 5a, the CG approaches of PR, LS, and DY in Figs. 5c, e, and f, respectively, seem to exhibit comparable to slightly poorer behavior. When applied to S, the CG technique of FR in Fig. 5b seems to have solely negative impacts on convergence to mG, and when used to Sc, it appears to have negative effects in general. As can be shown in Fig. 5g, the CG technique of CD produces negative consequences in S but no real impact in Sc. All three CG techniques shown in Fig. 5d–5i—the HZ and HS approaches shown in Fig. 5h and the L-BFGS technique shown in Fig. 5i—have positive outcomes. Some of these variations, when started from almost any of the 441 possible sites, converge to the global minimum.

Outlook

Using nonlinear conjugate gradient and limited-memory quasi-Newton updates with an optimum weighting of these updates, we have investigated the behavior of a well-liked phase retrieval lgorithm, Fienup's HIO, while updating an exit wave both within and outside the support. By analyzing a low-dimensional, synthetic issue, we were able to assess the approaches' resilience and see how these generalized updates might either aid or hinder convergence to an optimum solution. According to our findings, an algorithm's capability to recover the specified exit wave is greatly enhanced by using a mix of CG and L-BFGS updates. We have also shown that some combinations are not resilient and should be avoided.

Experimenters that use HIO often employ several initial speculations for the exit wave, perform multiple independent trials, and then compare the recovered exit waves. The resulting solutions are almost always novel, and the determination of what constitutes a "good" solution is frequently left to qualitative rather than quantitative measures. We expect that experimentalists' confidence in reducing the number of beginning points evaluated will grow upon applying the generalized modifications described here.

References

(Reference 1) Abbey, B.; Nugent, K.A.; Williams, G.J.; Lark, J.N.; Peele, A.G.; Pfeifer; de Jonge; and McNulty, I. Coherent diffractive imaging via a keyhole. 2008, Nature Physics 4, 394–398. Those authors are [2] H. H. Bauschke, P. L. Combettes, and D. R. Luke. A convex optimization perspective on phase retrieval, error reduction algorithms, and Fienup variations. Optical Society of America A, 2002, 19(7):1334-1345. For further information, see [3] by authors M. Dierolf, A. Menzel, P. Thibault, P. Schneider, C.M. Kewish, R. Wepf, O. Bunk, and F.

ISSN: 0976-0172

Journal of Bioscience And Technology
www.jbstonline.com

Pfeiffer. Nanoscale ptychographic x-ray computed tomography. 2010;467(7314):436-439 in Nature. Reference: [4] M. C. Ferris and J. S. Pang. Complementarity issues in engineering and economics. 1997, SIAM Review, Vol. 39, No. 4, pp. 669–713. A comparison of phase retrieval techniques, by J. R. Fienup, [5]. 1982's Appl. Optics 21(15):2758-2769. W. W. Hager and H. Zhang [6]. Conjugate-gradient techniques for nonlinear problems: a review. Pacific 2006, J. Optim. 2, 35–58. A. Marchesini, S. Optimization using phase retrieval and the saddle point. Journal of the Optical Society of America A, 2007;24(10):3289–3296. A.J. Wright and J. Nocedal. Optimization via Numerical Means. New York: Springer-Verlag, 1999. To wit: [9] D. Paganin. Optical Coherence Tomography for X-Rays. Press, Oxford, 2006. Sorber, Lathauwer, and Barel [10]. Optimization with no restrictions on the real or complex variables. 2012, SIAM Journal of Optimization, 22(3), pp.879-898. To cite this section: [11] A. Tripathi, J. Mohanty, S.H. Dietze, O.G. Shpyrko, E. Shipton, E.E. Fullerton, S.S. Kim, and I. McNulty. Imaging using dichroic coherent diffractometry. 108(33):13393-13398, 2011. Proc. Natl. Acad. Sci. SA.